UNIVERSIDADE DE SÃO PAULO
Instituto de Ciências Matemáticas e de Computação
ISSN 0103-2569

A Numerical Technique for Predicting Incompressible Turbulent Free-Surface Fluid Flow Problems

V.G. Ferreira
M.F. Tomé
J.A. Cuminato
A. Castelo
N. Mangiavacchi

Nº 168

RELATÓRIOS TÉCNICOS

São Carlos – SP
Mai./2002

A Numerical Technique for Predicting Incompressible Turbulent Free-Surface Fluid Flow Problems

V. G. FERREIRA[a], M. F. TOMÉ[b], J. A. CUMINATO[b]
A. CASTELO[b] and N. MANGIAVACCHI[b]

[a] *Departamento de Estatística, Matemática Aplicada e Computação*
IGCE – Instituto de Geociências e Ciências Exatas
Av. 24-A, 1515 - C.P. 178 - 13506-900, Rio Claro, SP, Brazil

[b] *Departamento de Ciências de Computação e Estatística*
ICMC – Instituto de Ciências Matemáticas e de Computação
Av. Trabalhador São Carlense, 400, C.P. 668, 13251-900, São Carlos, SP, Brazil

ABSTRACT

This report describes a computational method for the solution of incompressible turbulent free-surface fluid flow problems. The closure of the time-averaged Navier-Stokes equations is achieved by using two-equation $\kappa - \varepsilon$ turbulence model. In order to stabilize the numerical calculations, a high-order upwinding technique is adopted for the discretization of the non-linear derivatives. The flexibility of the method is demonstrated by application to several two-dimensional and axisymmetric fluid flows.

KEY WORDS: Computational Fluid Dynamics; Time-Averaged Navier-Stokes; Turbulence Modeling; Two-Equation $\kappa - \varepsilon$ Turbulence Model; High-Order Upwinding; Free-Surface Fluid Flow; Finite-Difference Formulation

1 Introduction

Numerical solutions of the time-averaged Navier-Stokes equations for turbulent flow field have received a great deal of attention in recent years, since, in principle, they describe fluid flow problems with any level of complexity. The only uncertanty in this approach is that introduced by turbulence model to effect closure of the mean conservation equations. The effects of the turbulence in the fluid flow sometimes play an important part in the physical process because of its increased mixing properties, which can affect the overall temperature, density and velocity distributions in the flow. However, compared to confined fluid flow problems, the numerical solution of turbulent free-surface fluid flow problems represents a challenge, since the free-surface itself is one of the unknowns.

The main purpose of this report is to present a computational technique for predicting incompressible turbulent free-surface fluid flow problems using two versions of the two-equation $\kappa-\varepsilon$ turbulence model. The numerical solution procedure is applied to a zero-pressure-gradient turbulent boundary-layer on a flat plate and jets impinging onto a flat surface.

2 Governing Equations

The conservation equations for time-dependent, viscous incompressible turbulent newtonian fluid flow are the time-averaged Navier-Stokes equations, the mass conservation equation, and the κ and ε transport equations

$$\frac{\partial u}{\partial t}+\frac{1}{r^\alpha}\frac{\partial(r^\alpha uu)}{\partial r}+\frac{\partial(uv)}{\partial z}=-\frac{\partial p_e}{\partial r}+\frac{1}{Re}\frac{\partial}{\partial z}\left(\frac{\partial u}{\partial z}-\frac{\partial v}{\partial r}\right)+\frac{1}{Fr^2}g_r$$
$$+\quad\frac{1}{Re}\left[2\frac{1}{r^\alpha}\frac{\partial}{\partial r}\left(r^\alpha\nu_t\frac{\partial u}{\partial r}\right)+\frac{\partial}{\partial z}\left(\nu_t\left(\frac{\partial u}{\partial z}+\frac{\partial v}{\partial r}\right)\right)-2\alpha\frac{\nu_t u}{r^{2\alpha}}\right], \tag{1}$$

$$\frac{\partial v}{\partial t}+\frac{1}{r^\alpha}\frac{\partial(r^\alpha vu)}{\partial r}+\frac{\partial(vv)}{\partial z}=-\frac{\partial p_e}{\partial z}-\frac{1}{Re}\frac{1}{r^\alpha}\frac{\partial}{\partial r}\left(r^\alpha\left(\frac{\partial u}{\partial z}-\frac{\partial v}{\partial r}\right)\right)+\frac{1}{Fr^2}g_z$$
$$+\quad\frac{1}{Re}\left[2\frac{\partial}{\partial z}\left(\nu_t\frac{\partial v}{\partial z}\right)+\frac{1}{r^\alpha}\frac{\partial}{\partial r}\left(r^\alpha\nu_t\left(\frac{\partial u}{\partial z}+\frac{\partial v}{\partial r}\right)\right)\right], \tag{2}$$

$$\frac{1}{r^\alpha}\frac{\partial(r^\alpha u)}{\partial r}+\frac{\partial v}{\partial z}=0, \tag{3}$$

$$\frac{\partial\kappa}{\partial t}+\frac{1}{r^\alpha}\frac{\partial(r^\alpha u\kappa)}{\partial r}+\frac{\partial(v\kappa)}{\partial z}=\frac{1}{Re}\left[\frac{1}{r^\alpha}\frac{\partial}{\partial r}\left(r^\alpha(1+\nu_t/\sigma_\kappa)\frac{\partial\kappa}{\partial r}\right)+\frac{\partial}{\partial z}\left((1+\nu_t/\sigma_\kappa)\frac{\partial\kappa}{\partial z}\right)\right]$$
$$+\quad P-\varepsilon, \tag{4}$$

$$\frac{\partial\varepsilon}{\partial t}+\frac{1}{r^\alpha}\frac{\partial(r^\alpha u\varepsilon)}{\partial r}+\frac{\partial(v\varepsilon)}{\partial z}=\frac{1}{Re}\left[\frac{1}{r^\alpha}\frac{\partial}{\partial r}\left(r^\alpha(1+\nu_t/\sigma_\varepsilon)\frac{\partial\varepsilon}{\partial r}\right)+\frac{\partial}{\partial z}\left((1+\nu_t/\sigma_\varepsilon)\frac{\partial\varepsilon}{\partial z}\right)\right]$$
$$+\quad(C_{1\varepsilon}P-C_{2\varepsilon}\varepsilon)/T_t+\beta E, \tag{5}$$

where t is the time, $u=u(r,z,t)$ and $v=v(r,z,t)$ are, respectively, the components in the r and z directions of the local time-averaged velocity vector field $\mathbf{u}=\mathbf{u}(r,z,t)$, $\kappa=\kappa(r,z,t)$ is the local time-averaged turbulent kinetic energy of the fluctuating motion, $\varepsilon=\varepsilon(r,z,t)$ is the dissipation of κ, $p_e=p+\frac{2}{3}\frac{1}{Re}\kappa$ is the effective scalar pressure field divided by the density, and $\mathbf{g}=(g_r,g_z)$ is the gravitational acceleration. The non-dimensional parameters $Re=U_0L_0/\nu$ and $Fr=U_0/\sqrt{L_0|\mathbf{g}|}$ denote the associated Reynolds and Froude numbers, respectively, in which U_0 is a characteristic velocity scale, L_0 is a length scale, and ν is the kinematic viscosity of the fluid. The isotropic eddy-viscosity ν_t, the turbulent shear stress production P, the time scale T_t, and the gradient dissipation E are, respectively, defined as

$$\nu_t=C_\mu f_\mu\kappa T_t, \tag{6}$$

$$P = \nu_t \left(2 \left(\frac{\partial u}{\partial r} \right)^2 + 2 \left(\frac{\partial v}{\partial z} \right)^2 + 2\alpha \left(\frac{u}{r^\alpha} \right)^2 + \left(\frac{\partial v}{\partial r} + \frac{\partial u}{\partial z} \right)^2 \right), \tag{7}$$

$$T_t = (1-\beta) Min \left\{ \frac{\kappa}{\varepsilon}, \frac{2}{3C_\mu} \sqrt{\frac{3}{8|\mathbf{S}|^2}} \right\} + \beta \left\{ \frac{\kappa}{\varepsilon} + \left(\frac{1}{\varepsilon} \right)^{1/2} \right\}, \tag{8}$$

$$E = \frac{2\nu_t}{Re} \left(\left(\frac{\partial^2 v}{\partial r^2} \right)^2 + \left(\frac{\partial^2 u}{\partial z^2} \right)^2 \right), \tag{9}$$

where, in Eq. (8), $|\mathbf{S}|^2 = \mathbf{D}:\mathbf{D}$, with $\mathbf{D} = \nabla\mathbf{u} + (\nabla\mathbf{u})^{\mathbf{T}}$. Together with the model constants C_μ, $C_{1\varepsilon}$, $C_{2\varepsilon}$, σ_κ and σ_ε, the parameter β in Eqs. (5) and (8) is used to specify the two-equation $\kappa-\varepsilon$ turbulence models considered in this work. In the case of $C_\mu = 0.09$, $C_{1\varepsilon} = 1.44$, $C_{2\varepsilon} = 1.92$, $\sigma_\kappa = 1.0$, $\sigma_\varepsilon = 1.3$ and $\beta = 0$, we deal with the standard high-Reynolds number form of the $\kappa - \varepsilon$ model [13] (named in this paper of HRe $\kappa - \varepsilon$ model), with the time scale proposed by Durbin [6] for appropriate treatment of stagnation-point anomaly. When the model constants are that proposed by Hoffman [11]; that is, $C_\mu = 0.09$, $C_{1\varepsilon} = 1.81$, $C_{2\varepsilon} = 2.0$, $\sigma_\kappa = 2.0$, $\sigma_\varepsilon = 3.0$ and $\beta = 1$, we treat with a low-Reynolds number form of the $\kappa - \varepsilon$ model (named here of LRe $\kappa - \varepsilon$ model), which is similar to that proposed by Yang and Shih [26].

The dumping function f_μ in Eq. (6) assumes the value $f_\mu = 1$ in the case of the HRe $\kappa - \varepsilon$ model, and takes the following expression in the case of the LRe $\kappa - \varepsilon$ model

$$f_\mu = \left(1 - Exp(-a_1 Re_{z_w} - a_3 Re_{z_w}^3 - a_5 Re_{z_w}^5) \right)^{1/2}, \tag{10}$$

where a_1, a_3 and a_5 are constants given by $a_1 = 1.5 \times 10^{-4}$, $a_3 = 5.0 \times 10^{-7}$, $a_5 = 1.0 \times 10^{-10}$ [26], and Re_{z_w} is the local Reynolds number defined as $Re_{z_w} = z_w Re \kappa^{1/2}$, z_w being the normal distance from the rigid-boundary to a point into the flow. The parameter α in Eqs. (1) through (7) is used to specify the coordinate system, namely: when $\alpha = 0$, plane cartesian coordinates are considered; and when $\alpha = 1$, cylindrical polar coodinates are assumed. Equations (1)-(8) have been nondimensionalized by the following transformations

$$u^* = uU_0, \quad r^* = rL, \quad v^* = vU_0, \quad z^* = zL, \quad t^* = tL/U_0, \quad g_i^* = g_i|\mathbf{g}|,$$

$$p_e{}^* = p_e U_0^2, \quad \kappa^* = \kappa\nu U_0/L, \quad \varepsilon^* = \varepsilon\nu U_0^2/L^2, \quad \nu_t{}^* = \nu_t\nu, \tag{11}$$

where variables with a star refer to their corresponding dimensional variables.

3 Initial and Boundary Conditions

Equations (1) through (5) are coupled, non-linear, partial differential equations and, together with the eddy-viscosity model (6), are sufficient, in principle, to solve for the five unknowns u, v, p_e, κ and ε when appropriated initial and boundary conditions are specified. In this work, a staggered mesh is used where the effective pressure, the turbulent kinetic energy and the dissipation rate are stored at the center of a computational grid cell, whereas velocities are

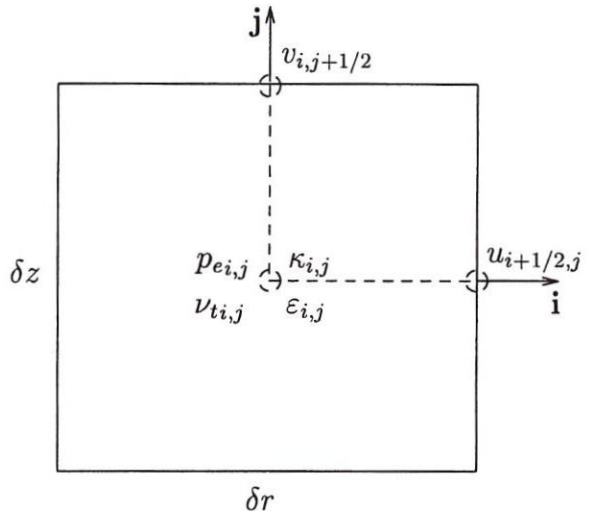

Figure 1: Staggered grid cell showing locations of the dependent variables.

stored at the cell edges. A typical cell showing the physical locations at which this dependent variables are defined is illustrated in Fig. 1. With this grid system, effective pressure boundary conditions are not needed. The initial and boundary conditions are implemented into the GENSMAC codes [18]–[19] as follows.

The initial conditions for the mean velocities and effective pressure are specified in the same way as in the laminar case [18]–[19]; that is, these variables are prescribed. It is difficult to specify initial conditions for turbulent variables since they must be in agreement with the physics of the problem. For the free-surface fluid flow problems considered in this work, we prescribe the initial conditions for κ and ε, and hence for ν_t, as functions of a turbulent intensity I [5], [23], and the large-scale characteristic velocity U_0. The variable κ is estimated by

$$\kappa = \kappa(I, U_0) = I{U_0}^2. \tag{12}$$

From dimensional reasoning, the variable ε is then determined as [15]

$$\varepsilon = \varepsilon(\kappa, l_t) = \frac{\kappa^{3/2}}{l_t}, \tag{13}$$

where l_t is a characteristic length associated to large scales and it is defined as $l_t = \bar{\beta}L$, being $\bar{\beta}$ constant. In non-dimensional form, Eqs. (12) and (13) can, respectively, be written as

$$\kappa = IRe \quad \text{and} \quad \varepsilon = \frac{1}{\bar{\beta}}\left(Re^{-1}\kappa^3\right)^{1/2}. \tag{14}$$

In all computations presented in this paper, $\bar{\beta} = 1.0 \times 10^{-2}$ and $I = 8.0 \times 10^{-2}$ were employed.

Five types of boundary conditions are implemented in this work, namely: inflow, outflow, symmetry, free-surface, and rigid-wall boundaries. At the inflow, the velocities u and v are

prescribed while the values of κ and ε are estimated consistently with the initial conditions (14). At the outflow, the streamwise gradient for each variable is required to be equal to zero. At symmetry boundaries, we are setting

$$u_n = 0, \quad \frac{\partial u_\tau}{\partial n} = 0, \quad \frac{\partial \kappa}{\partial n} = 0 \quad \text{and} \quad \frac{\partial \varepsilon}{\partial n} = 0, \tag{15}$$

where n and τ denote normal and tangential directions to the boundary, respectively. At the free-surface, we are considering that the fluid is moving into a passive atmosphere (zero-pressure) and, in the absence of surface tension forces, the normal and tangential components of the stress must be continuous across any free-surface, so that on such a surface we have (see, for example, Landau and Lifshitz [12])

$$\mathbf{n} \cdot (\sigma \cdot \mathbf{n}) = 0, \tag{16}$$

$$\mathbf{m} \cdot (\sigma \cdot \mathbf{n}) = 0. \tag{17}$$

Here, $\mathbf{n}$ and $\mathbf{m}$ are unit normal and tangent vectors to the surface, and σ is the general constitutive equation (Cauchy stress-tensor) defined as

$$\sigma = -p_e \mathbf{I} + Re^{-1}(1 + \nu_t)\mathbf{D}, \tag{18}$$

where $\mathbf{I}$ denotes the identity tensor. In the same way as is made in [19], the Eqs. (16) and (17) are applied by making accurate local finite-difference approximations on the free-surface: from condition (16) one determines the effective pressure; and from (17) one obtain the velocities at the free-surface. Due to the complexity of the dynamics of the turbulence near to the interface, the values of the turbulent variables κ and ε at the free-surface of the fluid are difficult to specify. For instance, it is not known how the turbulence interacts with the surface tension and, therefore, it is difficult to specify the distribution of κ on an irregular moving free-surface. So, as a first approximation, we assume that the free-surface is locally flat and the movement of the fluid does not cause discontinuity at this boundary. In summary, the turbulent variables at the free-surface are determined by imposing

$$\frac{\partial \kappa}{\partial n} = 0 \quad \text{and} \quad \frac{\partial \varepsilon}{\partial n} = 0. \tag{19}$$

The derivatives in Eq. (19) are approximated by first-order finite-differences.

The boundary conditions at rigid-wall depend on the $\kappa - \varepsilon$ viscosity model considered. When the simulation is performed with the HRe $\kappa - \varepsilon$ model, the wall-function approach is employed. In this case, the fundamental equation for determining the fictitious velocities and turbulent variables near a rigid-wall is the total wall shear stress τ_w given by [23]

$$\left(Re^{-1}(1 + \nu_t) \left| \frac{\partial \hat{u}}{\partial n} \right| \right) \Bigg|_{wall} \approx {u_\tau}^2 = \tau_w, \tag{20}$$

where $\hat{u}$ represents the velocity component tangential to the rigid-wall, and u_τ is the friction velocity. The values of the κ and ε in the inertial sublayer are, respectively, prescribed by well known relations

$$\kappa = Re \frac{\tau_w}{C_\mu^{1/2}} \quad \text{and} \quad \varepsilon = Re \frac{\tau_w u_\tau}{K z_w}, \tag{21}$$

where $K = 0.41$ is the von Kármán constant. In the viscous sublayer, we use the strategy of Sondak and Pletecher [17]; that is,

$$\kappa = Re\frac{\tau_w}{C_\mu^{1/2}}\left(\frac{z^+}{z_c{}^+}\right)^2 \quad \text{and} \quad \varepsilon = Re^{-1/2}\frac{\kappa^{3/2}}{l^*}, \tag{22}$$

where z^+ is defined as $z^+ = Reu_\tau z_w$, and l^* represents the length scale proposed by Norris and Reynolds [16]. Neglecting the buffer layer of a turbulent boundary-layer, the critic z^+ ($z_c{}^+$) in Eq. (22) delimits the viscous sublayer and the inertial sublayer. A detailed discussion of the initial and boundary conditions using the HRe $\kappa - \varepsilon$ turbulence model is given in Ferreira [8]. When the LRe $\kappa - \varepsilon$ model is used in the computations, the velocity at solid boundary is set to zero, in order to represent the no-slip velocity boundary conditions ($\mathbf{u} = \mathbf{0}$), and the values of the turbulent variables κ and ε at this boundary are, respectively, specified as [1]

$$\kappa = 0 \quad \text{and} \quad \varepsilon = 2Re^{-1}\left(\frac{\partial \kappa^{1/2}}{\partial n}\right)^2. \tag{23}$$

3.1 *Wall Functions Aspects*

It is well known that the HRe $\kappa-\varepsilon$ model requires modification for the simulation of flows near rigid boundaries, so as to account for damping of velocity flutuations and viscous effects. In general, the solution of the conservation equations in the inner layer of a turbulent boundary-layer is not necessary since the flow mechanism in such a region can be described reasonably well by employing wall-functions (for a more detailed discussion see, for example, Ferreira [8]). In what follows, we describe our implementation of wall-functions for the free-surface fluid flow treated in this paper.

The behavior of the mean velocity profiles in the viscous and inertial sublayers are, respectively, given by (see, for example, Refs. [3], [22] and [24])

$$u^+ - z^+ = 0, \tag{24}$$

$$ln(Ez^+) - Ku^+ = 0, \tag{25}$$

where $u^+ = \hat{u}/u_\tau$ and $E = exp(KB)$, B constant.

One of the central questions in the application of the wall-functions (20)-(22) is the accurate determination of the friction velocity, and hence the wall shear stress. It is determined from relation (24) or (25), depending on the local Reynolds number z^+. When u_τ is obtained by (25), the Newton-Raphson's method is applied with $u_\tau = 11.60$ as the initial condition. We initiate the calculations by determining the critic Reynolds number $z_c{}^+$, solution of the non-linear equation defined by the intersection of (24) and (25), and by imposing, in principle, that it is in the viscous sublayer. By neglecting the transition sublayer, in every cycle of the computational procedure, the friction velocity is estimated in the following manner: with the tangential velocity $\hat{u}$ known in the first grid cell adjacent to the wall, u_τ is updated according to the value of the z^+ given by (24). If z^+ is less than $z_c{}^+$, we use (24); on the other hand, we employ (25). The fictitious velocities are calculated by central-difference approximation of the Eq. (20) for a known wall shear stress.

4 Computational Procedure

The governing equations (1) through (5) are solved with an extension of the GENSMAC methodology for turbulent flow field (see Ferreira [8]). The detailed information of the GENSMAC code for laminar flow field is provided by Tomé and McKee [18] and Tomé et al. [19]. It is a finite-difference, explicit, first/second-order accurate numerical method based on a predictor-corrector scheme. By using a guessed effective pressure $\tilde{p}_e$ and an eddy-viscosity, the method consists of solving the time-averaged Navier-Stokes equations at the $(k+1)$ time-step for a tentative velocity field $\tilde{\mathbf{u}}$. The $\tilde{\mathbf{u}}$ velocity is related to the true velocity field $\mathbf{u}$, at the $(k+1)$ time-step, by an auxiliary potential function ψ which is calculated by a Poisson equation, originated by imposing $\nabla \cdot \mathbf{u} = 0$ at the $(k+1)$ time-step. The effective pressure and the turbulent variables κ and ε are then updated, and the procedure is repeated at each time-step. In particular, when calculating $\tilde{\mathbf{u}}$ in step 1, we employ an adaptive time-stepping routine (see Tomé and McKee [18]). The numerical solution procedure may be summarized as follows. It is supposed that, at a given time $t = t_0$, the velocity field $\mathbf{u}$ is known and suitable boundary conditions for the velocity and turbulent variables are given. Let $\tilde{p}_e(r,z,t)$ be an arbitrary effective pressure field, which satisfies the correct pressure condition on the free-surface. This pressure field is constructed employing the normal-stress condition (16) at the free-surface, and it is chosen arbitrarily (for instance $\tilde{p}_e(r,z,t) = 0$) into the fluid. The updated velocity field, the effective pressure and the turbulent variables, at time $t = t_0 + \delta t$, are calculated by the following steps:

1. With the eddy-viscosity ν_t known at $t = t_0$, compute an approximate velocity field $\tilde{\mathbf{u}}(r,z,t)$ from a finite-difference discretization of

$$\left.\frac{\partial \tilde{u}}{\partial t}\right|_{t=t_0} = \left\{ -\frac{1}{r^\alpha}\frac{\partial (r^\alpha uu)}{\partial r} - \frac{\partial (uv)}{\partial z} - \frac{\partial \tilde{p}_e}{\partial r} + \frac{1}{Re}\frac{\partial}{\partial z}\left(\frac{\partial u}{\partial z} - \frac{\partial v}{\partial r}\right) + \frac{1}{Fr^2} g_r \right.$$
$$\left. + \frac{1}{Re}\left[2\frac{1}{r^\alpha}\frac{\partial}{\partial r}\left(r^\alpha \nu_t \frac{\partial u}{\partial r}\right) + \frac{\partial}{\partial z}\left(\nu_t\left(\frac{\partial u}{\partial z} + \frac{\partial v}{\partial r}\right)\right) - 2\alpha\frac{\nu_t u}{r^{2\alpha}}\right] \right\}\Bigg|_{t=t_0}, \tag{26}$$

$$\left.\frac{\partial \tilde{v}}{\partial t}\right|_{t=t_0} = \left\{ -\frac{1}{r^\alpha}\frac{\partial (r^\alpha vu)}{\partial r} - \frac{\partial (vv)}{\partial z} - \frac{\partial \tilde{p}_e}{\partial z} - \frac{1}{Re}\frac{1}{r^\alpha}\frac{\partial}{\partial r}\left(r^\alpha \left(\frac{\partial u}{\partial z} - \frac{\partial v}{\partial r}\right)\right) + \frac{1}{Fr^2} g_z \right.$$
$$\left. + \frac{1}{Re}\left[2\frac{\partial}{\partial z}\left(\nu_t \frac{\partial v}{\partial z}\right) + \frac{1}{r^\alpha}\frac{\partial}{\partial r}\left(r^\alpha \nu_t \left(\frac{\partial u}{\partial z} + \frac{\partial v}{\partial r}\right)\right)\right] \right\}\Bigg|_{t=t_0}, \tag{27}$$

with $\tilde{\mathbf{u}}(r,z,t_0) = \mathbf{u}(r,z,t_0)$ using the correct boundary conditions for $\mathbf{u}(r,z,t_0)$. It can be shown (see, for example, Ferreira [8]) that $\tilde{\mathbf{u}}(r,z,t)$ possesses the correct vorticity at time t but does not satisfy (3), in general. By writting

$$\mathbf{u}(r,z,t) = \tilde{\mathbf{u}}(r,z,t) - \nabla\psi(r,z,t) \tag{28}$$

and imposing

$$\nabla^2\psi(r,z,t) = \nabla \cdot \tilde{\mathbf{u}}(r,z,t), \tag{29}$$

a velocity field is obtained in which the vorticity and mass are conserved;

2. Solve the Poisson equation (29). The appropriate boundary conditions for this elliptic equation are homogeneous Dirichlet-type on the free-surface and homogeneous Neumann-type on fixed boundaries [2]. These are treated in a similar way as in the GENSMAC code of Tomé and McKee [18] and Tomé et al. [19];

3. Calculate the velocity field $\mathbf{u}(r, z, t)$ from (28);

4. Compute the effective pressure. It can be shown (see Ferreira [8]) that this pressure field is given by

$$p_e(r, z, t) = \tilde{p}_e(r, z, t) + \psi(r, z, t)/\delta t; \tag{30}$$

5. Compute the kinetic energy κ from a finite-difference approximation of (4);

6. Compute the dissipation rate ε from a finite-difference approximation of (5);

7. Update the eddy-viscosity ν_t from (6);

8. Particle movement. The last step in the calculation involves the movement of the marker particles to their new positions. These are virtual particles (without mass, volume, or other properties), whose coordinates are stored and updated at the end of each cycle by solving the ordinary differential equations

$$\dot{r} = u(r, z, t) \quad \text{and} \quad \dot{z} = v(r, z, t) \tag{31}$$

by Euler's method. This provides a particle with its new coordinates, allowing us to determine whether or not it has moved into a new computational cell, or if it has left the containment region through an outflow-boundary. Update the boundary conditions and go back to the first step.

5 Discretization of the Governing Equations

In the solution procedure described in the previous section, the differential equations are discretized, using a finite-difference formulation on a uniform staggered grid, in time and space in precisely the same manner for all dependent variables. Particularly, the temporal derivatives are discretized using the first-order forward difference, while the spatial derivatives are approximated with standard second-order central differences, with the exception of the convective terms (named here of $CONV(\cdot)$), which are handled with the VONOS (Variable-Order Non-Oscillatory) scheme of Varonos and Bergeles [20]: a high-order accurate upwinding scheme, which satisfy the Convection Boundedness Criterion (CBC) proposed by Gaskell and Lau [10]. The VONOS scheme has the property of reducing unphysical numerical oscillations and, at the same time, minimizing the effects of artificial numerical diffusion. A detailed discussion of this convection scheme would go beyond the scope of this paper, and the reader is referred to Ferreira et al. [7] for details of implementation and application in laminar free-surface flows. The Poisson equation (29) is discretized using the usual five-point Laplacian operator, and the corresponding symmetric-positive definite linear system is solved by the conjugate-gradient method. In summary, the fluid flow equations (1)-(5) take the following discretized form:

• **r-Momentun:**

$$\tilde{u}^{n+1}_{i+1/2,j} = u^n_{i+1/2,j} + \delta t\Big\{ CONV(u)|_{i+1/2,j} - (p_{ei+1,j} - p_{ei,j})/\delta r$$

$$+\frac{1}{R_e\delta z}\Big[\Big((u_{i+1/2,j+1} - u_{i+1/2,j})/\delta z - (v_{i+1,j+1/2} - v_{i,j+1/2})/\delta r\Big)$$

$$-\Big((u_{i+1/2,j} - u_{i+1/2,j-1})/\delta z - (v_{i+1,j-1/2} - v_{i,j-1/2})/\delta r\Big)\Big]$$

$$+\frac{2}{R_e r^{\alpha}_{i+1/2,j}\delta r^2}\Big(r^{\alpha}_{i+1,j}\nu_{ti+1,j}(u_{i+3/2,j} - u_{i+1/2,j}) - r^{\alpha}_{i,j}\nu_{t_{i,j}}(u_{i+1/2,j} - u_{i-1/2,j})\Big)$$

$$+\frac{1}{R_e\delta z}\Big[\nu_{ti+1/2,j+1/2}\Big((u_{i+1/2,j+1} - u_{i+1/2,j})/\delta z + (v_{i+1,j+1/2} - v_{i,j+1/2})/\delta r\Big)$$

$$-\nu_{ti+1/2,j-1/2}\Big((u_{i+1/2,j} - u_{i+1/2,j-1})/\delta z + (v_{i+1,j-1/2} - v_{i,j-1/2})/\delta r\Big)\Big]$$

$$-\frac{2\alpha}{R_e r^{2\alpha}_{i+1/2,j}}\nu_{ti+1/2,j}u_{i+1/2,j} + \frac{1}{F_r^2}g_r\Big\}^n, \tag{32}$$

where

$$CONV(u)\Big|^n_{i+1/2,j} = \Big[\frac{1}{r^{\alpha}}\frac{\partial(r^{\alpha}uu)}{\partial r} + \frac{\partial(uv)}{\partial z}\Big]\Big|^n_{i+1/2,j}; \tag{33}$$

• **z-Momentun:**

$$\tilde{v}^{n+1}_{i,j+1/2} = v^n_{i,j+1/2} + \delta t\Big\{ CONV(v)|_{i,j+1/2} - (p_{ei,j+1} - p_{ei,j})/\delta z$$

$$-\frac{1}{R_e\delta r r^{\alpha}_{i,j+1/2}}\Big[r^{\alpha}_{i+1/2,j+1/2}\Big((u_{i+1/2,j+1} - u_{i+1/2,j})/\delta z - (v_{i+1,j+1/2} - v_{i,j+1/2})/\delta r\Big)$$

$$-r^{\alpha}_{i-1/2,j+1/2}\Big((u_{i-1/2,j+1} - u_{i-1/2,j})/\delta z - (v_{i,j+1/2} - v_{i-1,j+1/2})/\delta r\Big)\Big]$$

$$+\frac{2}{R_e\delta z^2}\Big(\nu_{ti,j+1}(v_{i,j+3/2} - v_{i,j+1/2}) - \nu_{ti,j}(v_{i,j+1/2} - v_{i,j-1/2})\Big)$$

$$+\frac{1}{R_e\delta r r^{\alpha}_{i,j+1/2}}\Big[r^{\alpha}_{i+1/2,j+1/2}\nu_{t_{i+1/2,j+1/2}}\Big((u_{i+1/2,j+1} - u_{i+1/2,j})/\delta z + (v_{i+1,j+1/2} - v_{i,j+1/2})/\delta r\Big)$$

$$-r^{\alpha}_{i-1/2,j+1/2}\nu_{ti-1/2,j+1/2}\Big((u_{i-1/2,j+1} - u_{i-1/2,j})/\delta z + (v_{i,j+1/2} - v_{i-1,j+1/2})/\delta r\Big)\Big]$$

$$+\frac{1}{F_r^2}g_z\Big\}^n, \tag{34}$$

where

$$CONV(v)\Big|_{i,j+1/2}^{n} = \left[\frac{1}{r^{\alpha}}\frac{\partial(r^{\alpha}vu)}{\partial r} + \frac{\partial(vv)}{\partial z}\right]\Bigg|_{i,j+1/2}^{n}; \tag{35}$$

• **Poisson Equation for ψ:**

$$\frac{1}{r_{i,j}^{\alpha}\delta r^2}\left(r_{i+1/2,j}^{\alpha}(\psi_{i+1,j}-\psi_{i,j}) - r_{i-1/2,j}^{\alpha}(\psi_{i,j}-\psi_{i-1,j})\right) + (\psi_{i,j+1} - 2\psi_{i,j} + \psi_{i,j-1})/\delta z^2$$

$$= \frac{1}{r_{i,j}^{\alpha}\delta r}(r_{i+1/2,j}^{\alpha}\tilde{u}_{i+1/2,j} - r_{i-1/2,j}^{\alpha}\tilde{u}_{i-1/2,j}) + (\tilde{v}_{i,j+1/2} - \tilde{v}_{i,j-/12})/\delta z, \tag{36}$$

• **κ-Equation:**

$$\kappa_{i,j}^{n+1} = \kappa_{i,j}^{n} + \delta t\left\{CONV(\kappa)|_{i,j} + \frac{1}{R_e r_{i,j}^{\alpha}\delta r^2}\left[r_{i+1/2,j}^{\alpha}(1+(\nu_{ti+1,j}+\nu_{ti,j})/2\sigma_{\kappa})(\kappa_{i+1,j}-\kappa_{i,j})\right.\right.$$

$$-r_{i-1/2,j}^{\alpha}(1+(\nu_{ti,j}+\nu_{ti-1,j})/2\sigma_{\kappa})(\kappa_{i,j}-\kappa_{i-1,j})\Big] + \frac{1}{Re\delta z^2}\Big[(1+(\nu_{ti,j+1}+\nu_{ti,j})/2\sigma_{\kappa})(\kappa_{i,j+1}-\kappa_{i,j})$$

$$\left.\left.-(1+(\nu_{ti,j}+\nu_{ti,j-1})/2\sigma_{\kappa})(\kappa_{i,j}-\kappa_{i,j-1})\Big] + P_{i,j} - \epsilon_{i,j}\right\}^{n}, \tag{37}$$

where

$$CONV(\kappa)\Big|_{i,j}^{n} = \left[\frac{1}{r^{\alpha}}\frac{\partial(r^{\alpha}u\kappa)}{\partial r} + \frac{\partial(v\kappa)}{\partial z}\right]\Bigg|_{i,j}^{n}; \tag{38}$$

• **ε-Equation:**

$$\varepsilon_{i,j}^{n+1} = \varepsilon_{i,j}^{n} + \delta t\left\{CONV(\varepsilon)|_{i,j} + \frac{1}{R_e r_{i,j}^{\alpha}\delta r^2}\left[r_{i+1/2,j}^{\alpha}(1+(\nu_{ti+1,j}+\nu_{ti,j})/2\sigma_{\varepsilon})(\varepsilon_{i+1,j}-\varepsilon_{i,j})\right.\right.$$

$$-r_{i-1/2,j}^{\alpha}(1+(\nu_{ti,j}+\nu_{ti-1,j})/2\sigma_{\varepsilon})(\varepsilon_{i,j}-\varepsilon_{i-1,j})\Big] + \frac{1}{Re\delta z^2}\Big[(1+(\nu_{ti,j+1}+\nu_{ti,j})/2\sigma_{\varepsilon})(\varepsilon_{i,j+1}-\varepsilon_{i,j})$$

$$-(1+(\nu_{ti,j}+\nu_{ti,j-1})/2\sigma_{\varepsilon})(\varepsilon_{i,j}-\varepsilon_{i,j-1})\Big] + (C_{1\varepsilon}P_{i,j} - C_{2\varepsilon}\varepsilon_{i,j})/T_{i,j} +$$

$$\alpha 2\frac{\nu_{ti,j}}{Re}\left[\frac{1}{4\delta r^4}\left(v_{i+1,j+1/2} + v_{i+1,j-1/2} - 2(v_{i,j+1/2}+v_{i,j-1/2}) + v_{i-1,j+1/2} + v_{i-1,j-1/2}\right)^2\right.$$

$$\left.\left.+\frac{1}{4\delta z^4}\left(u_{i+1/2,j+1} + u_{i-1/2,j+1} - 2(u_{i+1/2,j}+u_{i-1/2,j}) + u_{i+1/2,j-1} + u_{i-1/2,j-1}\right)^2\right]\right\}^{n} \tag{39}$$

where

$$CONV(\varepsilon)\Big|_{i,j}^{n} = \left[\frac{1}{r^{\varepsilon}}\frac{\partial(r^{\alpha}u\varepsilon)}{\partial r} + \frac{\partial(v\varepsilon)}{\partial z}\right]\Bigg|_{i,j}^{n}; \tag{40}$$

The eddy-viscosity, the production of turbulence, the gradient dissipation, and the time scale are, respectively, discretized as

$$\nu_{t\,i,j}^{n} = C_{\mu} f_{\mu} \kappa_{i,j}^{n} T_{i,j}^{n}; \tag{41}$$

$$\begin{aligned} P_{i,j}^{n} = \nu_{i,j}^{n} \Bigg\{ 2 \Bigg[& \frac{1}{\delta r^2} (u_{i+1/2,j} - u_{i-1/2,j})^2 + \frac{1}{\delta z^2} (v_{i,j+1/2} - v_{i,j-1/2})^2 + \left(\frac{u_{i+1/2,j} + u_{i-1/2,j}}{2 r_{i,j}^{\alpha}} \right)^2 \Bigg] \\ & + \Bigg[\frac{1}{4\delta z} \left(u_{i+1/2,j+1} + u_{i-1/2,j+1} - u_{i+1/2,j-1} - u_{i-1/2,j-1} \right) \\ & + \frac{1}{4\delta r} \left(v_{i+1,j+1/2} + v_{i+1,j-1/2} - v_{i-1,j+1/2} - v_{i-1,j-1/2} \right) \Bigg]^2 \Bigg\}^{n}; \end{aligned} \tag{42}$$

$$\begin{aligned} E = \frac{2\nu_{t\,i,j}^{n}}{Re} \Bigg\{ & \frac{1}{4\delta r^4} \left(v_{i+1,j+1/2} + v_{i+1,j-1/2} - 2(v_{i,j+1/2} + v_{i,j-1/2}) + v_{i-1,j+1/2} + u_{i-1,j-1/2} \right)^2 \\ & + \frac{1}{4\delta z^4} \left(u_{i+1/2,j+1} + u_{i-1/2,j+1} - 2(u_{i+1/2,j} + u_{i-1/2,j}) + u_{i+1/2,j-1} + u_{i-1/2,j-1} \right)^2 \Bigg\}^{n}; \end{aligned} \tag{43}$$

$$T_{t\,i,j}^{n} = (1-\beta) Min \left\{ \frac{\kappa_{i,j}^{n}}{\varepsilon_{i,j}^{n}}, \frac{2}{3C_{\mu}} \sqrt{\frac{3}{8|\mathbf{S}|^2}} \right\} + \beta \left\{ \frac{\kappa_{i,j}^{n}}{\varepsilon_{i,j}^{n}} + \left(\frac{1}{\varepsilon_{i,j}^{n}} \right)^{1/2} \right\}. \tag{44}$$

5.1 *Discretization of the Convective Terms*

We now consider the use of the high-order upwinding VONOS scheme for the discretization of the convective terms in the transport equations. It should be pointed out that, based on the local velocity direction of the flow, this composite differencing scheme is a good compromise between numerical stability and accuracy. For brevity, only the discretizations of two non-linear derivatives are presented; all the other convective derivatives are treated similarly (for more details, see [8]).

Let us consider, for example, the convective terms (33) and (38). Then, these terms can be, respectively, written as

$$\left[\frac{1}{r^{\alpha}} \frac{\partial (r^{\alpha} uu)}{\partial r} + \frac{\partial (uv)}{\partial z} \right] \Bigg|_{i+1/2,j}^{n} = \left[\frac{1}{r^{\alpha}{}_{i+1/2,j}} \frac{\partial (r^{\alpha} uu)}{\partial r} \Bigg|_{i+1/2,j} + \frac{\partial (uv)}{\partial z} \Bigg|_{i+1/2,j} \right]^{n}, \tag{45}$$

$$\left[\frac{1}{r^{\alpha}} \frac{\partial (r^{\alpha} u\kappa)}{\partial r} + \frac{\partial (v\kappa)}{\partial z} \right] \Bigg|_{i,j}^{n} = \left[\frac{1}{r^{\alpha}{}_{i,j}} \frac{\partial (r^{\alpha} u\kappa)}{\partial r} \Bigg|_{i,j} + \frac{\partial (v\kappa)}{\partial z} \Bigg|_{i,j} \right]^{n}, \tag{46}$$

where the non-linear derivatives are approximated by

$$\left.\frac{\partial(r^{\alpha}uu)}{\partial r}\right|_{i+1/2,j} \approx [r^{\alpha}{}_{i+1,j}(\bar{u}_{i+1,j}u_{i+1,j}) - r^{\alpha}{}_{i,j}(\bar{u}_{i,j}u_{i,j})]/\delta r, \tag{47}$$

$$\left.\frac{\partial(uv)}{\partial z}\right|_{i+1/2,j} \approx (\bar{v}_{i+1/2,j+1/2}u_{i+1/2,j+1/2} - \bar{v}_{i+1/2,j-1/2}u_{i+1/2,j-1/2})/\delta z, \tag{48}$$

$$\left.\frac{\partial(r^{\alpha}u\kappa)}{\partial r}\right|_{i,j} \approx [r^{\alpha}{}_{i+1/2,j}(\bar{u}_{i+1/2,j}\kappa_{i+1/2,j}) - r^{\alpha}{}_{i-1/2,j}(\bar{u}_{i-1/2,j}\kappa_{i-1/2,j})]/\delta r, \tag{49}$$

$$\left.\frac{\partial(v\kappa)}{\partial z}\right|_{i,j} \approx (\bar{v}_{i,j+1/2}\kappa_{i,j+1/2} - \bar{v}_{i,j-1/2}\kappa_{i,j-1/2})/\delta z. \tag{50}$$

The convective velocities in Eqs. (47)-(50) are obtained as

$$\bar{u}_{i+1,j} = 0.5(u_{i+3/2,j} + u_{i+1/2,j}), \quad \bar{v}_{i+1/2,j+1/2} = 0.5(v_{i+1,j+1/2} + v_{i,j+1/2}),$$

$$\bar{u}_{i,j} = 0.5(u_{i+1/2,j} + u_{i-1/2,j}), \quad \bar{v}_{i+1,j-1/2} = 0.5(v_{i+1,j-1/2} + v_{i,j-1/2}),$$

$$\bar{u}_{i+1/2,j} = u_{i+1/2,j}, \quad \bar{u}_{i-1/2,j} = u_{i-1/2,j},$$

$$\bar{v}_{i,j+1/2} = v_{i,j+1/2}, \quad \bar{v}_{i,j-1/2} = v_{i,j-1/2}.$$

In Eqs. (47)-(50), the transported properties u and κ at grid points $(i+1,j)$, (i,j), $(i+1/2,j+1/2)$, $(i+1/2,j-1/2)$ and $(i+1/2,j)$, $(i-1/2,j)$, $(i,j+1/2)$, $(i,j-1/2)$, respectively, are approximated by using the upwinding VONOS scheme. For example, the velocity u at the point $(i+1/2,j+1/2)$ and the kinetic energy κ at the point $(i+1/2,j)$ are, respectively, approximated by

$$u_{i+1/2,j+1/2} \approx (1-S_1)\left\{\begin{array}{ll} u_{i+\frac{1}{2},j}\,, & \text{if } \widehat{u}_{i+1/2,j} \notin [0,\ 1] \\ 10u_{i+\frac{1}{2},j} - 9u_{i+\frac{1}{2},j-1}\,, & \text{if } \widehat{u}_{i+1/2,j} \in [0,\ 3/74) \\ \frac{3}{8}u_{i+\frac{1}{2},j+1} + \frac{6}{8}u_{i+\frac{1}{2},j} - \frac{1}{8}u_{i+\frac{1}{2},j-1}\,, & \text{if } \widehat{u}_{i+1/2,j} \in [3/74,\ 1/2) \\ 1.5u_{i+\frac{1}{2},j} - 0.5u_{i+\frac{1}{2},j-1}\,, & \text{if } \widehat{u}_{i+1/2,j} \in [1/2,\ 2/3) \\ u_{i+\frac{1}{2},j+1}\,, & \text{if } \widehat{u}_{i+1/2,j} \in [2/3,\ 1] \end{array}\right\}$$

$$+S_1\left\{\begin{array}{ll} u_{i+\frac{1}{2},j+1}\,, & \text{if } \widehat{u}_{i+1/2,j+1} \notin [0,\ 1] \\ 10u_{i+\frac{1}{2},j+1} - 9u_{i+\frac{1}{2},j+2}\,, & \text{if } \widehat{u}_{i+1/2,j+1} \in [0,\ 3/74) \\ \frac{3}{8}u_{i+\frac{1}{2},j} + \frac{6}{8}u_{i+\frac{1}{2},j+1} - \frac{1}{8}u_{i+\frac{1}{2},j+2}\,, & \text{if } \widehat{u}_{i+1/2,j+1} \in [3/74,\ 1/2) \\ 1.5u_{i+\frac{1}{2},j+1} - 0.5u_{i+\frac{1}{2},j+2}\,, & \text{if } \widehat{u}_{i+1/2,j+1} \in [1/2,\ 2/3) \\ u_{i+\frac{1}{2},j}\,, & \text{if } \widehat{u}_{i+1/2,j+1} \in [2/3,\ 1] \end{array}\right\},$$

$$\kappa_{i+1/2,j} \approx (1-S_2)\left\{\begin{array}{l}\kappa_{i,j}\ , \quad \text{if } \widehat{\kappa}_{i,j} \notin [0,\ 1] \\ 10\kappa_{i,j} - 9\kappa_{i-1,j}\ , \quad \text{if } \widehat{\kappa}_{i,j} \in [0,\ 3/74) \\ \frac{3}{8}\kappa_{i+1,j} + \frac{6}{8}\kappa_{i,j} - \frac{1}{8}\kappa_{i-1,j}\ , \quad \text{if } \widehat{\kappa}_{i,j} \in [3/74,\ 1/2) \\ 1.5\kappa_{i,j} - 0.5\kappa_{i-1,j}\ , \quad \text{if } \widehat{\kappa}_{i,j} \in [1/2,\ 2/3) \\ \kappa_{i+1,j}\ , \quad \text{if } \widehat{\kappa}_{i,j} \in [2/3,\ 1]\end{array}\right\}$$
$$+S_2\left\{\begin{array}{l}\kappa_{i+1,j}\ , \quad \text{if } \widehat{\kappa}_{i+1,j} \notin [0,\ 1] \\ 10\kappa_{i+1,j} - 9\kappa_{i+2,j}\ , \quad \text{if } \widehat{\kappa}_{i+1,j} \in [0,\ 3/74) \\ \frac{3}{8}\kappa_{i,j} + \frac{6}{8}\kappa_{i+1,j} - \frac{1}{8}\kappa_{i+2,j}\ , \quad \text{if } \widehat{\kappa}_{i+1,j} \in [3/74,\ 1/2) \\ 1.5\kappa_{i+1,j} - 0.5\kappa_{i+2,j}\ , \quad \text{if } \widehat{\kappa}_{i+1,j} \in [1/2,\ 2/3) \\ \kappa_{i,j}\ , \quad \text{if } \widehat{\kappa}_{i+1,j} \in [2/3,\ 1]\end{array}\right\},$$

where the parameters S_1 and S_2 are given by

$$S_1 = \begin{cases} 0, \text{ if } \bar{u}_{i+1/2,j+1/2} \geq 0 \\ 1, \text{ otherwise} \end{cases}, \quad S_2 = \begin{cases} 0, \text{ if } \bar{u}_{i+1/2,j} \geq 0 \\ 1, \text{ otherwise} \end{cases}$$

and the normalized variables $\widehat{u}_{i+1/2,j}$, $\widehat{u}_{i+1/2,j+1}$, $\widehat{\kappa}_{i,j}$ and $\widehat{\kappa}_{i+1,j}$ are defined as [14]

$$\widehat{u}_{i+1/2,j} = \frac{u_{i+\frac{1}{2},j} - u_{i+\frac{1}{2},j-1}}{u_{i+\frac{1}{2},j+1} - u_{i+\frac{1}{2},j-1}}, \quad \widehat{u}_{i+1/2,j+1} = \frac{u_{i+\frac{1}{2},j+1} - u_{i+\frac{1}{2},j+2}}{u_{i+\frac{1}{2},j} - u_{i+\frac{1}{2},j+2}},$$

$$\widehat{\kappa}_{i,j} = \frac{\kappa_{i,j} - \kappa_{i-1,j}}{\kappa_{i+1,j} - \kappa_{i-1,j}}, \quad \widehat{\kappa}_{i+1,j} = \frac{\kappa_{i+1,j} - \kappa_{i+2,j}}{\kappa_{i,j} - \kappa_{i+2,j}}.$$

6 Results and Discussions

A two-dimensional zero-pressure-gradient turbulent boundary-layer over a flat plate is first used to validate the numerical technique. This fluid flow problem has frequently appeared in the literature, and several methods have been proposed to estimate the skin-friction coefficient C_f [9]. For this problem, the Reynolds number based on the inflow velocity $U_0 = 1.0$ m/s and the channel height $H = 1.0$ m is $Re = 2.0 \times 10^6$. Three different meshes are used, namely: the coarse mesh (20×100 computational cells, $\delta x = \delta y = 0.05$ m); the medium mesh (40×200 computational cells, $\delta x = \delta y = 0.025$ m); and the fine mesh (80×400 computational cells, $\delta x = \delta y = 0.0125$ m). In what follows, we present three well established estimates to this coefficient and the numerical estimate given by the GENSMAC code adapted with the HRe $\kappa - \varepsilon$ model.

Figure 2 illustrates a comparison between the dimensionless turbulent skin-friction coefficient profiles $C_f = 2\tau_w$, as a function of the local Reynolds number $Re_x = U_0 x/\nu$, obtained by the HRe $\kappa - \varepsilon$ model, in the three meshes and at the non-dimensional time $t = 6.477$, and the estimates given by Prandtl, power-law and White (see, for example, White [24] for details). In this picture, for simple comparison, the laminar profile is also presented. As shown in Figs. 2 a), b) and c), the numerical estimates are generally satisfactory for Re_x beyond 1.0×10^6.

It can also be observed from Fig. 2 d) that when the coarse mesh is twice refined, there was convergence of the numerical solution for a profile near the power-law and White profiles. On the other hand, for $Re_x \leq 1.0 \times 10^6$, the discrepancy may be due to the uniform meshes used and the initial velocity profile not being sufficiently turbulent at the entrance region. Of course, near to $Re_x = 1.0 \times 10^6$, it may be noticed the tendency of the numerical profile, in the fine mesh (Fig. 2 c)), to follow the theoretical profiles.

In order to investigate the performance of the numerical method where the turbulent stress is predominant, we fix the non-dimensional position $x = 3.75$ at the plate and extract the velocity profile $u^+ = u^+(lnz^+)$, at this point, using the numerical solution in the medium mesh. This profile was then compared with experimental data of Wieghardt and Tillmann [25] and two profiles derived by variation of the constants K and B in the law (25). One these profiles, proposed by Nikuradse and Prandtl (see, for instance, [24]), assumes the values $K = 0.40$ and $B = 5.50$, and the other, estimated by Coles and Hirst [4], uses the values $K = 0.41$ and $B = 5.00$. Figure 3 presents a comparison these two profiles and some experimental data with the computed profile. One can see, from this picture, that the results indicate compatibility between these data and profiles, and the numerical solution in the turbulent wake, showing that the efective stress tensor estimated at the wall correctly transfers its effects to regions where $z^+ > 500$. This confirms that the numerical solution, using the HRe $\kappa - \varepsilon$ model, simulates reasonably well the effects of the turbulence in regions remote to the rigid boundary.

Results with both the HRe $\kappa - \varepsilon$ and LRe $\kappa - \varepsilon$ models will be now examined for a two-dimensional jet impinging onto a flat surface. For this free-surface fluid flow problem, the Reynolds number based on the inflow velocity $U_0 = 2.0$ m/s and inflow diameter $D = 1.0 \times 10^{-2}$ m is $Re = 3.2 \times 10^4$, and the Froude number is $F_r = U_0/\sqrt{gD} = 6.39$. Three different meshes are also used for this free-surface flow, namely: the coarse mesh (25×50 computational cells, $\delta x = \delta y = 0.002$ m); the medium mesh (50×200 computational cells, $\delta x = \delta y = 0.001$ m); and the fine mesh (100×400 computational cells, $\delta x = \delta y = 0.0005$ m). In the following, a quantitative comparison between two-dimensional Watson's analytical predictions [21] and numerical results will be performed. Figure 4 shows a comparison between the variation of the non-dimensional free-surface height $h/0.5D$ with non-dimensional distance $(x/0.5D)Re^{-1/4}$, obtained by the HRe $\kappa - \varepsilon$ (Figs. 4 a), c) and e) - left column) and LRe $\kappa - \varepsilon$ (Figs. 4 b), d) and f) - right column) models in the three meshes and at the non-dimensional time $t = 38.0$, and approximate viscous and inviscid two-dimensional solutions by Watson [21]. In this picture, for simple information, Watson's boundary-layer thickness is also presented. It can be seen, from Fig. 4 (left column) and Fig. 5 a), that the calculations using the HRe $\kappa - \varepsilon$ model on fine mesh (200×400 grid points) provide, practically, the same results as those obtained in the coarse and medium meshes, indicating grid independence of the numerical results. One can note also that the numerical results on the coarse and medium meshes monotonicaly converge to the numerical solution on the fine mesh, and that the numerical solution on the fine mesh is in good agreement with the Watson's viscous solution.

At the same non-dimensional time of the simulation with the HRe $\kappa - \varepsilon$ model, the comparison between the free-surface height obtained from the LRe $\kappa - \varepsilon$ model and the Watson's viscous solution was also made, and the results are displayed in the Fig. 4 (right column) and Fig. 5 b). It is obvious that the numerical results with this turbulence model on the three meshes are

unsatisfactory. We believe that, for this specific fluid flow problem, the disagreement between viscous analytical solution, developed by Watson, and the numerical solution, obtained by the $LRe\ \kappa-\varepsilon$ model, may be attributed to the fact that the numerical solution has been calculated on a uniform mesh, resulting in a poor resolution of the viscous sublayer. In fact, for this high Reynolds number flow, the viscous sublayer of the turbulent boundary-layer is so thin that it is time consuming to use enough grid points to solve it.

Next, results with both the $HRe\ \kappa-\varepsilon$ and $LRe\ \kappa-\varepsilon$ models will be examined for an axisymmetric jet impinging onto a flat surface. For this problem, the Reynolds number based on the inflow velocity $U_0 = 1.0$ m/s and inflow diameter $D = 0.02$ m is $Re = \frac{\pi}{2}U_0 D/\nu = 5.03 \times 10^4$, and the Froude number is $F_r = U_0/\sqrt{gD} = 2.26$. For this free-surface flow, three different meshes are also used which will be referred to as the coarse (50×100 computational cells, $\delta r = \delta z = 0.001$ m), medium (100×200 computational cells, $\delta r = \delta z = 0.0005$ m), and fine (200×400 computational cells, $\delta r = \delta z = 0.00025$ m) meshes. In the following, a quantitative comparison between axisymmetric Watson's analytical predictions [21] and numerical results will be performed. Figure 6 displays a comparison between the variation of the non-dimensional free-surface height $(h/0.5D)Re^{1/9}$ with non-dimensional distance $(r/0.5D)Re^{-1/9}$, obtained from the $HRe\ \kappa-\varepsilon$ (Figs. 6 a), c) and e) - left column) and $LRe\ \kappa-\varepsilon$ (Figs. 6 b), d) and f) - right column) models in the three meshes and at the non-dimensional time $t = 20.48$, and approximate general viscous and inviscid axisymmetric solutions by Watson [21]. It can be seen, from the left column of this picture, that the numerical solutions using the $HRe\ \kappa-\varepsilon$ model on coarse and medium meshes monotonicaly converge to the numerical solution on the fine mesh, and the numerical solution on the fine mesh shows reasonable agreement with the Watson's viscous solution.

At the same non-dimensional time of the simulation with the $HRe\ \kappa-\varepsilon$ model, the comparison between the surface height obtained from the $LRe\ \kappa-\varepsilon$ model and the Watson's viscous solution was also made, and the results are displayed in the right column of the Fig. 6. It is clear that the numerical results with this turbulence model on coarse and medium meshes are unsatisfactory, whereas the solution on the fine mesh converges to a solution near Watson's viscous solution. As in the two-dimensional calculations, a possible explanation of the discrepancy between the viscous analytical solution developed by Watson and the numerical solution obtained by the $LRe\ \kappa-\varepsilon$ model is attributed to the poor resolution of the viscous sublayer. On the other hand, the discrepancy between the viscous solution of Watson and the $HRe\ \kappa-\varepsilon$ model may be attributed to Watson's hypotheses to obtain his analytical solutions. In fact, the approximate general viscous solution, according to Watson, is in disagreement with experimental data.

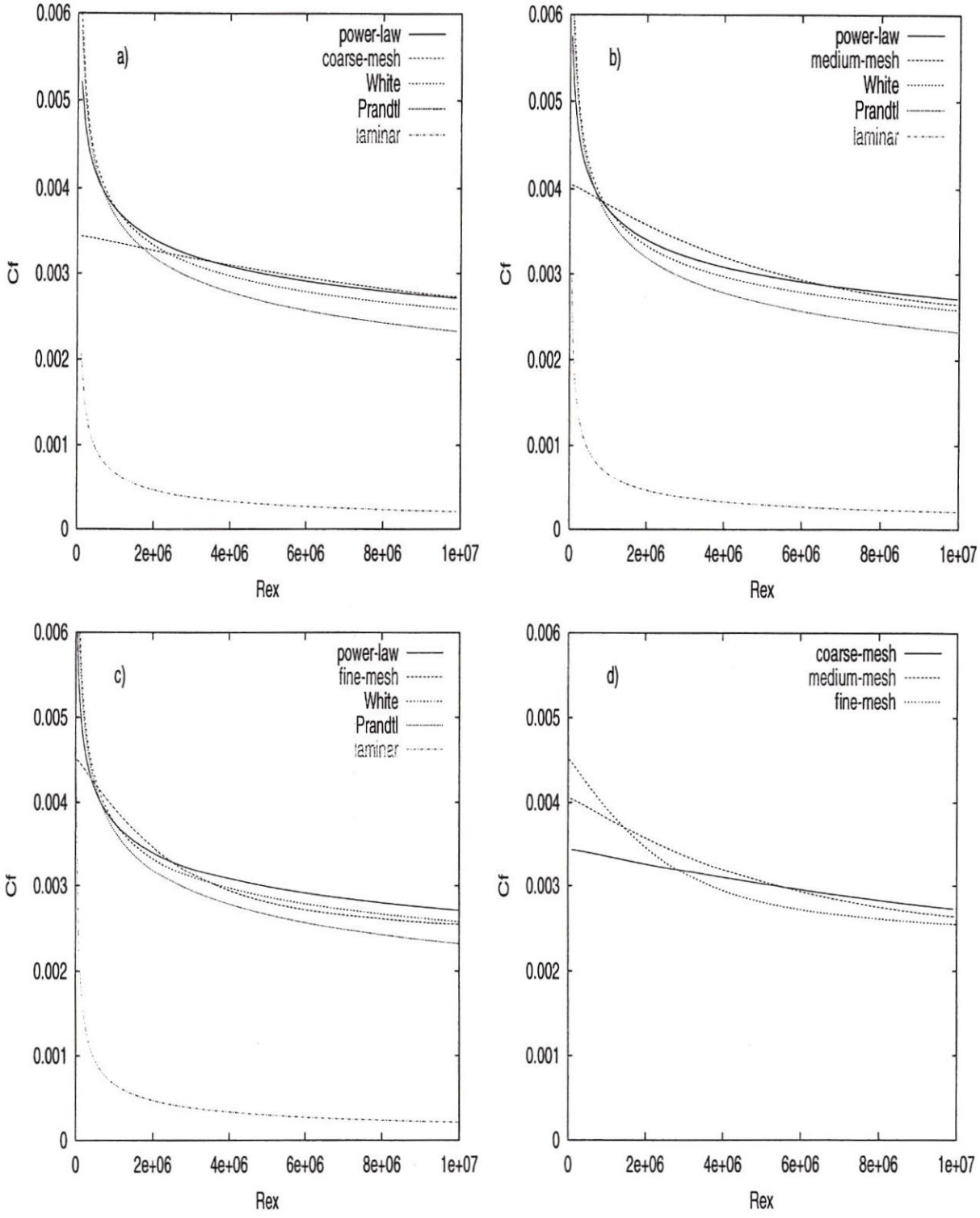

Figure 2: Comparison between the skin-friction coefficient profiles $C_f = C_f(Re_x)$ for the turbulent boundary-layer on a flat plate, showing theoretical estimates and that by HRe $\kappa - \varepsilon$ model: a) Comparison in the coarse mesh; b) Comparison in the medium mesh; c) Comparison in the fine mesh; d) Comparison of the three numerical solutions.

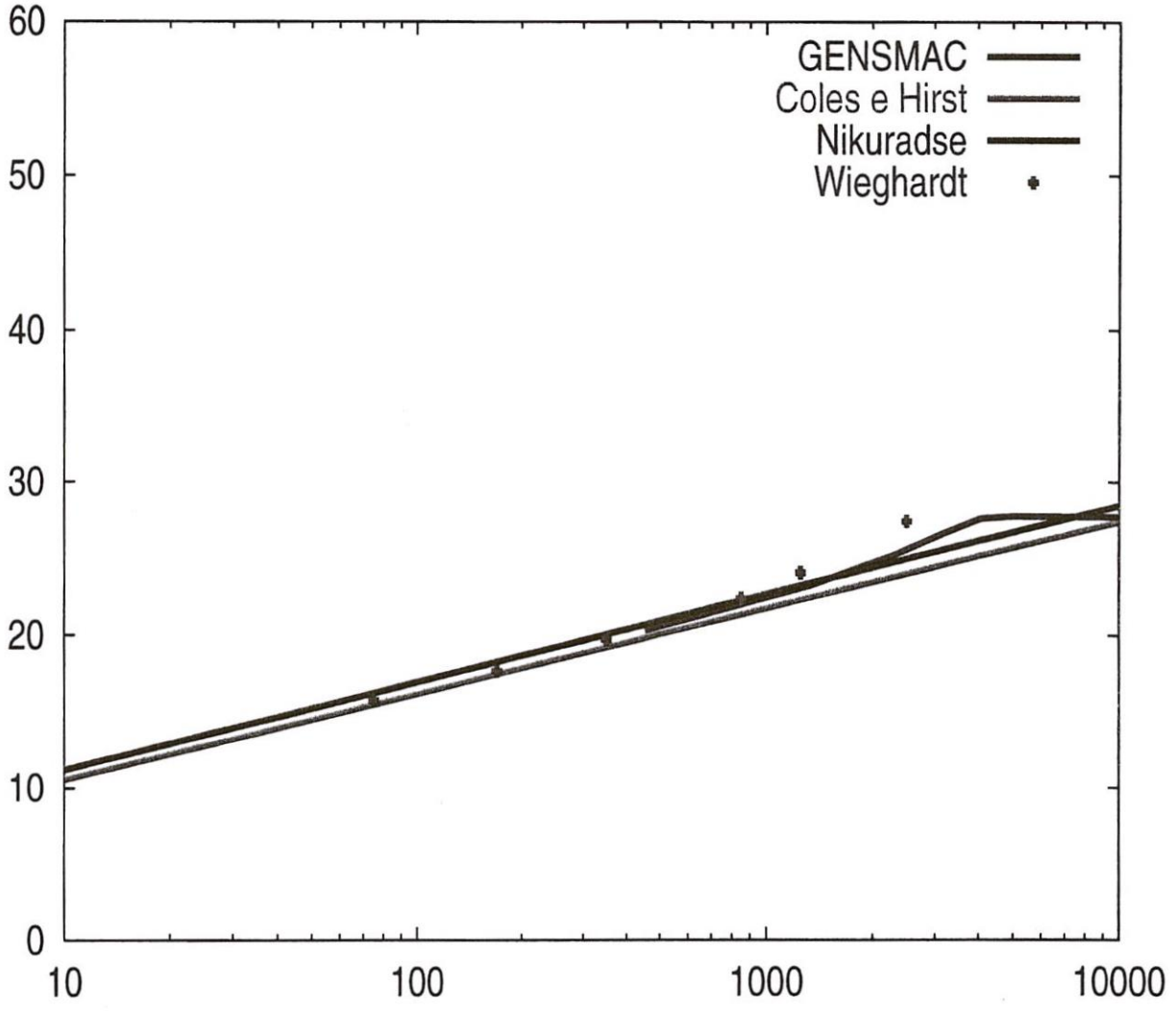

Figure 3: Profile of the velocity in the turbulent boundary-layer, showing the comparison between the numerical solution, two profiles derived of the of law (25) and some experimental data of Wieghardt and Tillmann.

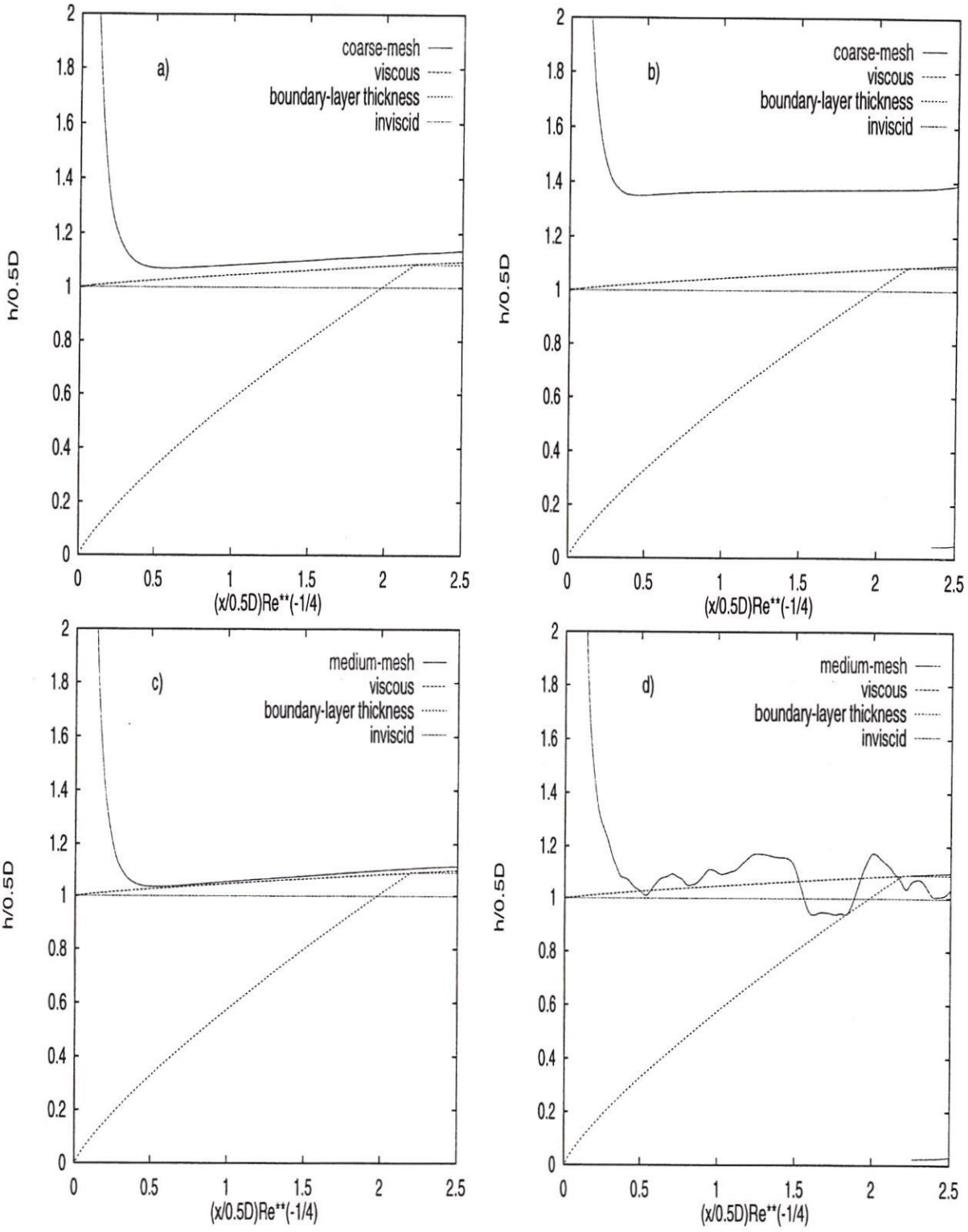

Figure 4: Comparison between the free-surface height obtained by two-dimensional HRe $\kappa-\varepsilon$ (left column) and LRe $\kappa-\varepsilon$ (right column) models and approximate analytical solutions by Watson.

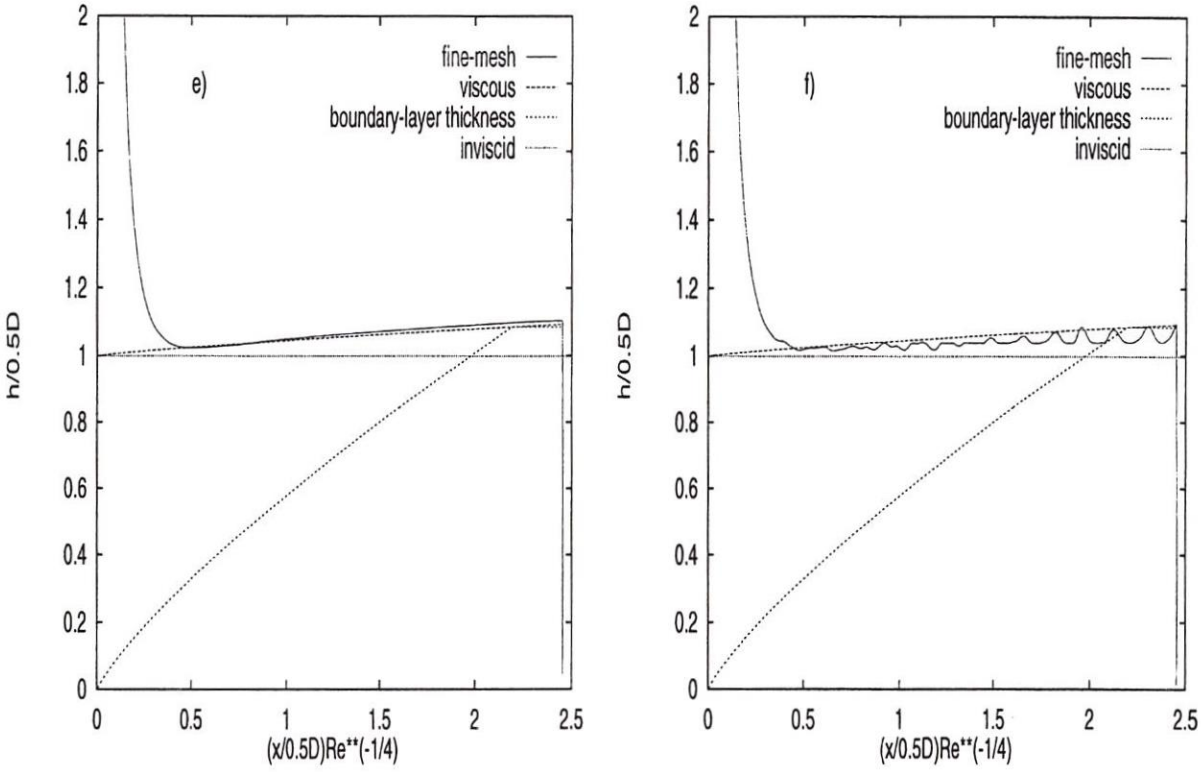

Figure 4: Continued

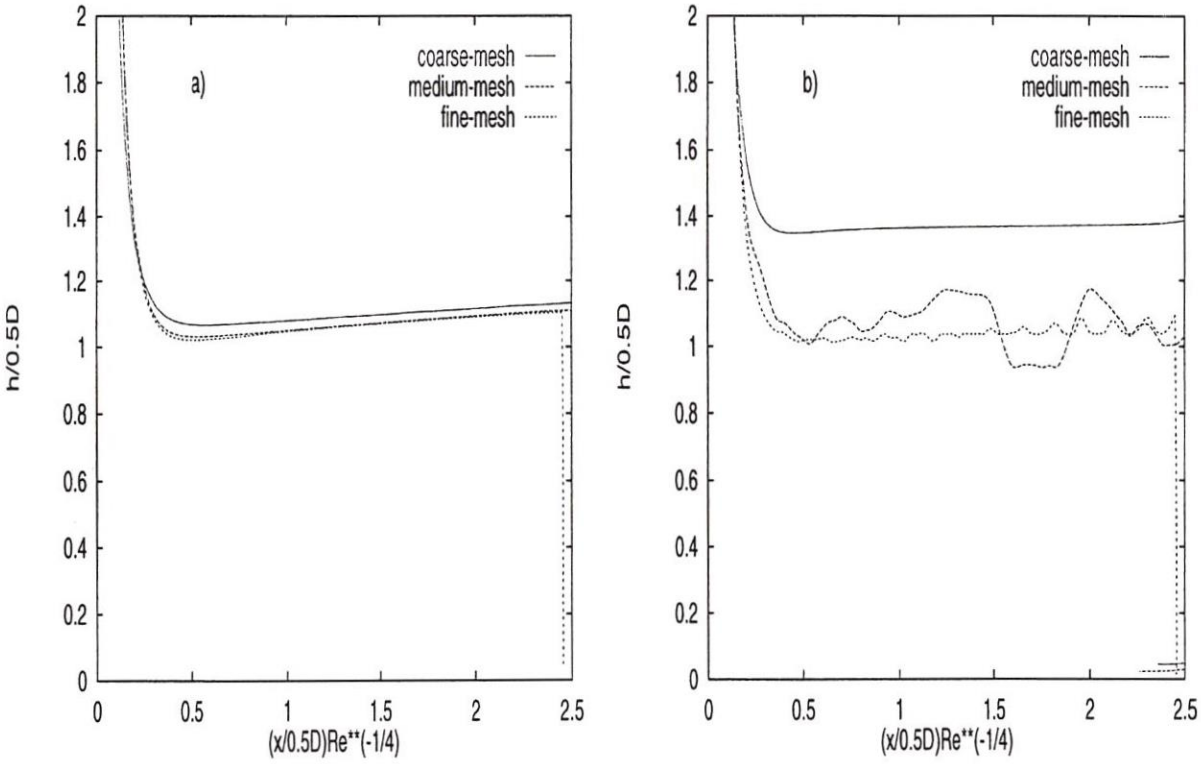

Figure 5: Comparison between of the three numerical solutions and viscous solution of Watson: a) $HRe\ \kappa - \varepsilon$ model; b) $LRe\ \kappa - \varepsilon$ model.

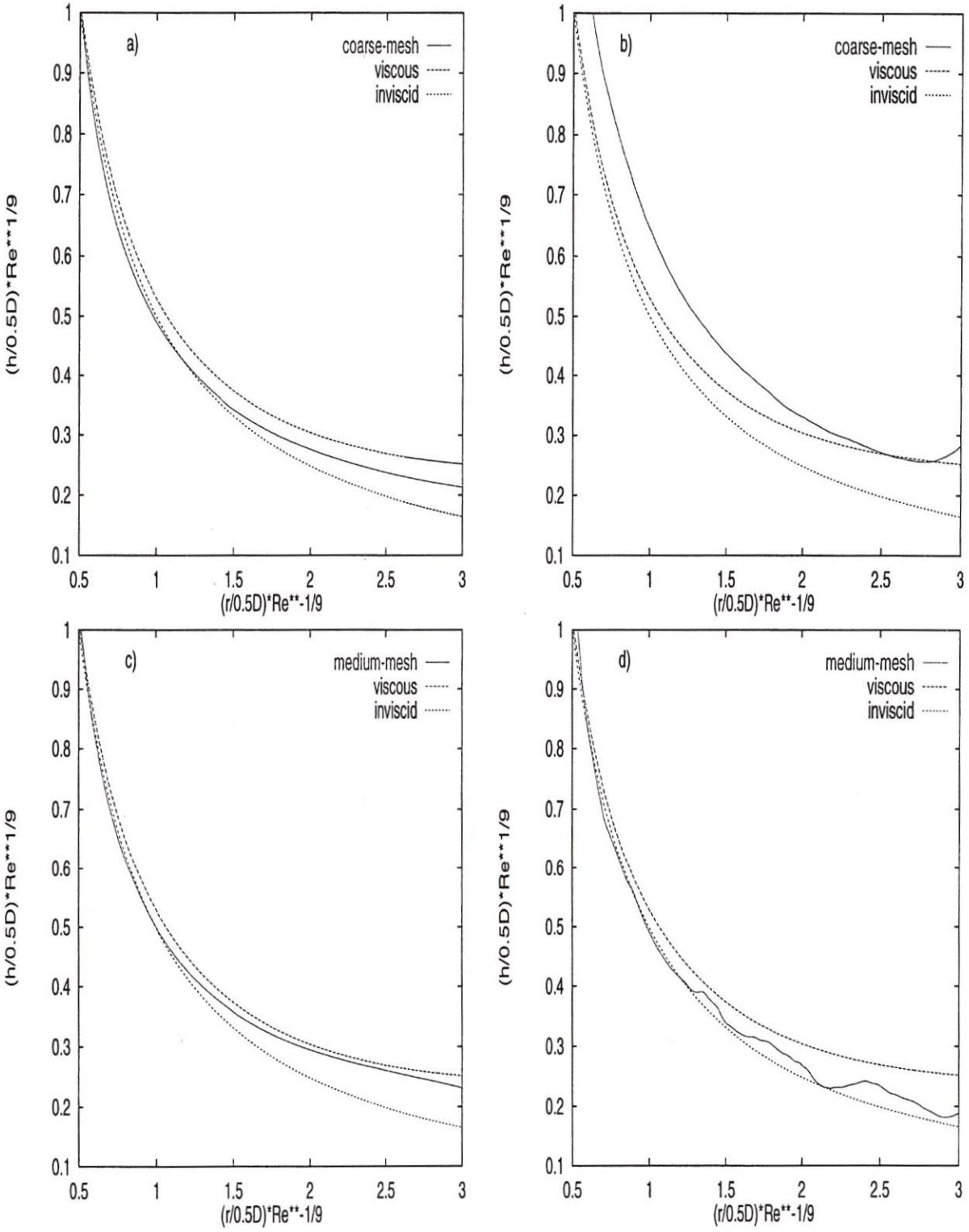

Figure 6: Comparison between the free-surface height obatined by axisymmetric $HRe\ \kappa - \varepsilon$ (left column) and $LRe\ \kappa - \varepsilon$ (right column) models and approximate analytical solutions by Watson.

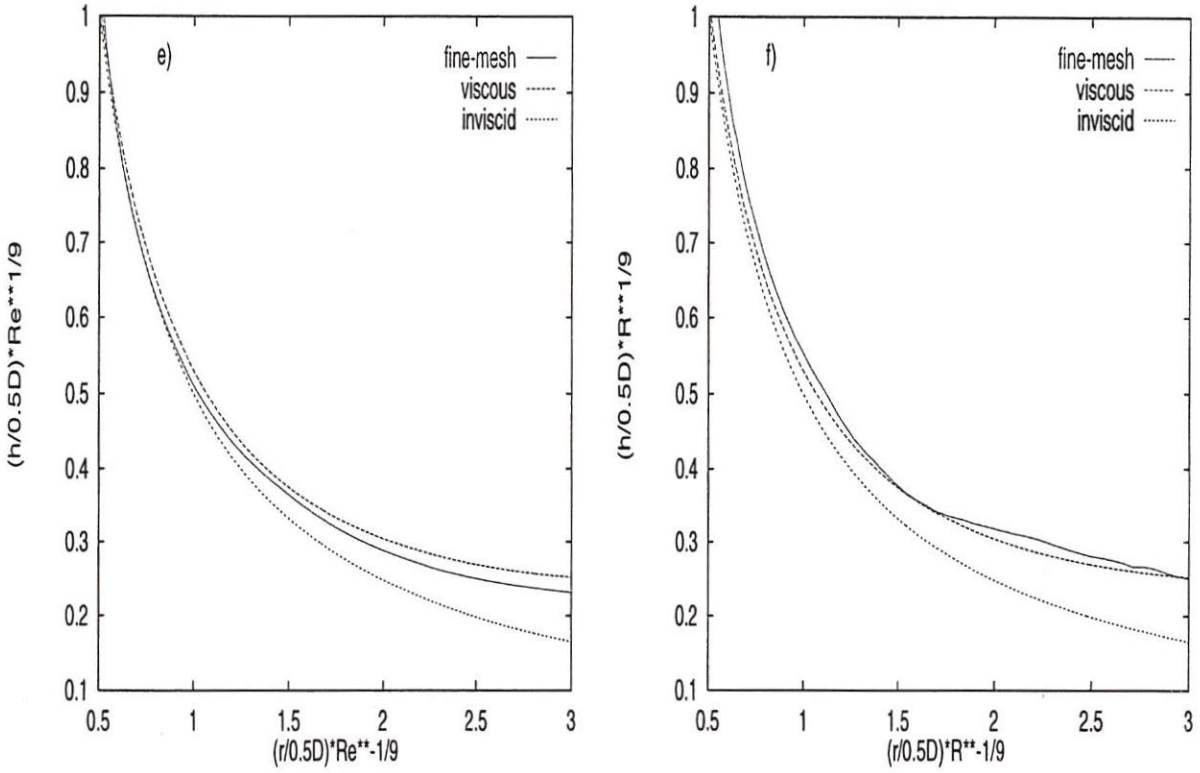

Figure 6: Continued

7 Conclusion

A finite-difference numerical method has been presented for the solution of turbulent free-surface fluid flow problems by using two versions of the $\kappa - \varepsilon$ turbulent models. In order to describe the turbulent effects on the mean flow, the κ and ε conservation equations were analysed and implemented into the two-dimensional and axisymmetric GENSMAC codes.

In an attempt to ensure bounded transient solutions during the course of iterations, the convection VONOS scheme was adopted for all non-linear derivatives of the convective transport equations. The numerical results show that it is beneficial to incorporate this high-order upwinding method in order to reduce the effects of numerical diffusion in turbulent free-surface flow problems.

According to the numerical results, the HRe $\kappa - \varepsilon$ model yields favorable predictions of zero-pressure-gradient turbulent boundary-layer on a flat plate and jet impingement flows. On the other hand, the numerical results using the LRe $\kappa - \varepsilon$ model were unsatisfactory. In terms of computational cost, it is important to note that when the $\kappa - \varepsilon$ viscosity model was applied with wall-functions the computer cost was reduced by approximately a factor of 3.

In order to include more physics in the turbulence modeling, the authors are looking at adaptation of the RNG (Renormalization Group Method) and Realizable $\kappa - \varepsilon$ models.

8 Acknowledgments

We gratefully acknowledge the support given by FAPESP (Fundação de Amparo à Pesquisa do Estado de São Paulo) and CNPq (Conselho Nacional de Desenvolvimento Científico e Tecnológico). The first author would like to acknowledge support from the DEMAC/IGCE/UNESP.

References

[1] Abe, K., Kondoh, T. and Nagano, Y., A new turbulence model for predicting fluid flow and heat transfer in separating and reattaching flows–I. Flow field calculations, *Int. J. Heat Mass Transfer*, **37**, 139-151 (1994).

[2] Amsden, A.A. and Harlow, F.H., A numerical technique for calculating incompressible fluid flow, *Report LA-4370, Los Alamos Laboratory* (1971).

[3] Bradshaw, P., "Turbulence", Topics in Applied Physics V. 12, Springer-Verlag (1976).

[4] Coles, D.E. and Hirst, E.A., Computation of turbulent boundary layer, *AFOSRIFFP Stanford Conference*, Porc. 1968 Conf. vol. 2, Stanford Univ. (1968).

[5] Costa, J.J., Oliveira, L.A. and Blay, D., Test of several versions for the $\kappa-\epsilon$ type turbulence modelling of internal mixed convection flows, *Int. J. Heat Mass Transfer*, **42**, 4391-4409 (1999).

[6] Durbin, P.A., On the $\kappa - \varepsilon$ stagnation point anomaly, *J. Heat and Fluid Flow*, **17**, 89-90 (1996).

[7] Ferreira, V.G., Tomé, M.F., Mangiavacchi, N., Castelo, A., Cuminato, J.A., Fortuna, A.O. and McKee, S., High order upwinding and the hydraulic jump, *Int. J. Numer. Meth. Fluids* (in press).

[8] Ferreira, V.G., Análise e implementação de esquemas de convecção e modelos de turbulência para simulação de escoamentos incompressíveis envolvendo superfícies livres, *Tese de Doutorado*, 177 p., ICMC-USP, São Carlos (2001).

[9] Ferziger, J.H., Lyrio, A.A., and Bardina, J.G., New skin friction and entrainment correlations for turbulent boundary layers, *J. Fluids Engrg.*, **104**, 407-544 (1982).

[10] Gaskell, P.H. and Lau, A.K.C., Curvature-compensated convective transport: SMART, a new boundedness-preserving transport algorithm, *Int. J. Numer. Meth. Fluids*, **8**, 617-641 (1988).

[11] Hoffman, G., Improved form of the low Reynolds number $\kappa - \varepsilon$ turbulence model, *Phys. Fluids*, **18**, 309-312 (1975).

[12] Landau, L.D. and Lifshitz, E.M., "Fluid Mechanics", Course of Theoretical Plysics V. 6, Butterworth-Heinemann, Great Britain (1975).

[13] Lauder, B.E. and Spalding, D.B., The numerical computation of turbulent flows, *Int. J. Numer. Meths. Fluids*, **15**, 127-146 (1974).

[14] Leonard, B.P., Simple high-accuracy resolution program for convective modelling of discontinuities, *Int. J. Numer. Meths. Fluids*, **8**, 1291-1318 (1988).

[15] Nagano, Y. and Tagawa, M., An improved $\kappa - \epsilon$ model for boundary layer flow, *ASME J. Fluids Engrg.*, **112**, 33-39 (1990).

[16] Norris, H.L. and Reynolds, W.C., Turbulent channel flow with a moving wavy boundary, *Stanford Univ. Dept. Mech. Eng.*, **TR TF-7** (1975).

[17] Sondak, D.L. and Pletcher, R.H., Application of wall functions to generalized nonorthogonal curvilinear coordinate systems, *AIAA J.*, **33**, 33-41 (1995).

[18] Tomé, M.F. and McKee, S., GENSMAC: A computational marker-and-cell method for free surface flows in general domains, *J. Comput. Phys.*, **110**, 171–186 (1994).

[19] Tomé, M.F., Castelo, A., Murakami, J., Cuminato, J.A., Minghim, R., Oliveira, C.F., Mangiavacchi, N. and McKee, S., Numerical simulation of axisymmetric free surface flows, *J. Comput. Phys.*, **157**, 441-472 (2000).

[20] Varonos, A. and Bergeles, G., Development and assessment of a variable-order non-oscillatory scheme for convection term discretization, *Int. J. Numer. Meths. Fluids*, **26**, 1-16 (1998).

[21] Watson, E.J., The radial spread of a liquid jet over a horizontal plane, *J. Fluid Mech.*, **20**, *part 3*, 481-499 (1964).

[22] Wilcox, D.C., Reassessment of the scale-setermining squation for advanced turbulence models, *AIAA J.*, **26**, 1299-1310 (1988).

[23] Wilcox, D.C., "Turbulence modeling for CFD, DCW Industries", Inc., California (1993).

[24] White, F.M., "Viscous fluid flow", McGraw-Hill, New York (1991).

[25] Wieghardt, K. and Tillmann, W., On the turbulent friction layer for rising pressure, *NACA Thechinical Memo.*, **1314** (1951).

[26] Yang, Z., and Shih, H., New time scale based $\kappa - \varepsilon$ model for near-wall turbulence, *AIAA J.*, **7**, 1191-1198 (1993).